4.6.3 Plate Dents

Type P dents are classified as plate dents. The shape of the Type P indenter is a flat square plate with a width of 24 in. This indenter shape is the same as the one used in the experimental program by Fowler. This is the largest indenter modeled. Type P dents were modeled on 12 in. and 36 in. diameter pipes. A model plot of indentation of a 15 percent *d/D* Type P dent is given in Fig. 4-114.

Type P dents have the most rebound of all the dent types modeled. The large flat indenter creates a flat dent without the curvature surrounding the contact region as found with other dent types. Thus, the dented shape does not provide any stiffness against rebound as compared to the other dent types. The change in dent shape from indentation through final rebound is given in Fig. 4-115 for a 10 percent *d/D* Type P dent in Pipe 12-2. Half of the initial dent depth is lost during initial rebound. After pressurization, approximately one fourth of the initial dent depth remains. As with longitudinal dent types, the maximum dent depth is located at the end of the contact region. The bulging rebound behavior is not noticed for Type P dents due to the large contact area. The entire dented area has similar rebound characteristics.

The cross section displaced shape for the model in Fig. 4-115 is given in Fig. 4-116 for the stages of rebound. At indentation, the cross section is elliptical in shape as with the other dent types. The large indenter size does not cause localized deformation as with the other dent types. Thus, Type P dents have more global deformation at indentation causing more horizontal displacement to an elliptical shape as compared to the other dent types.

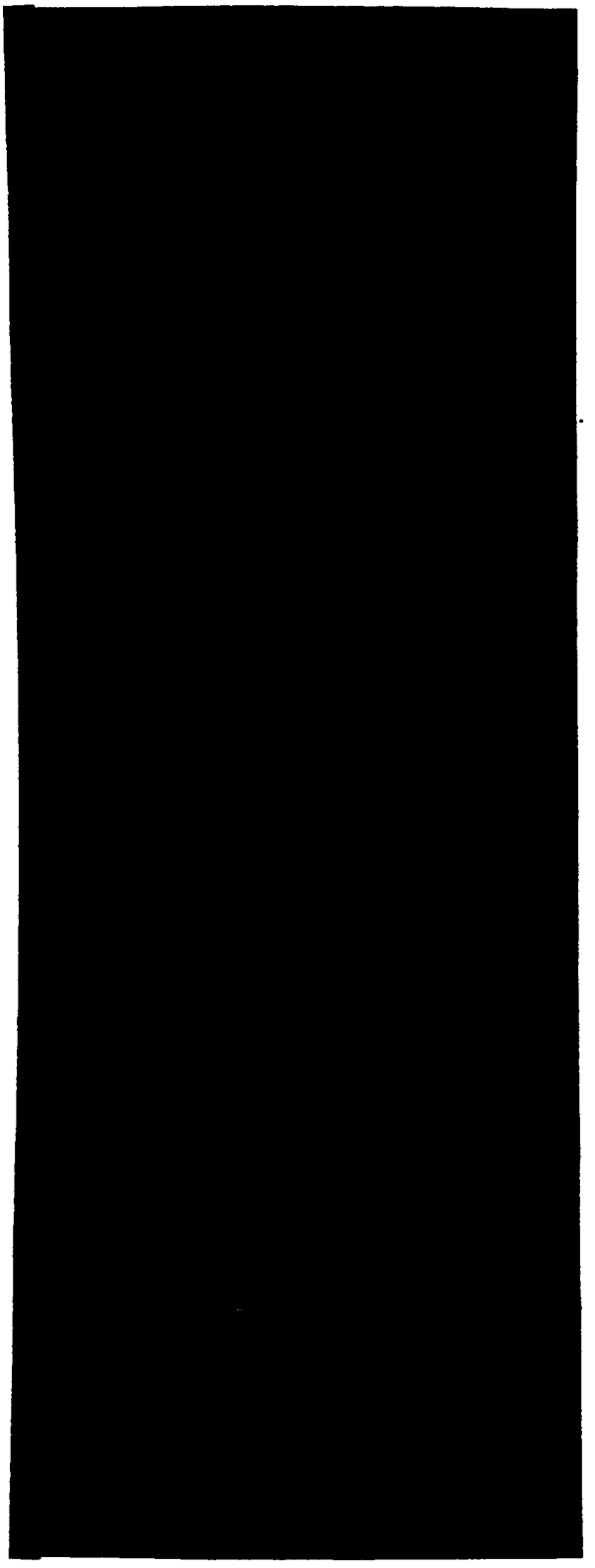

24 in.

Pipe! 18-3
Initial d/D = 15%
Dent Type P

Figure 4-114: Dent Type P Model Plot of Indentation.

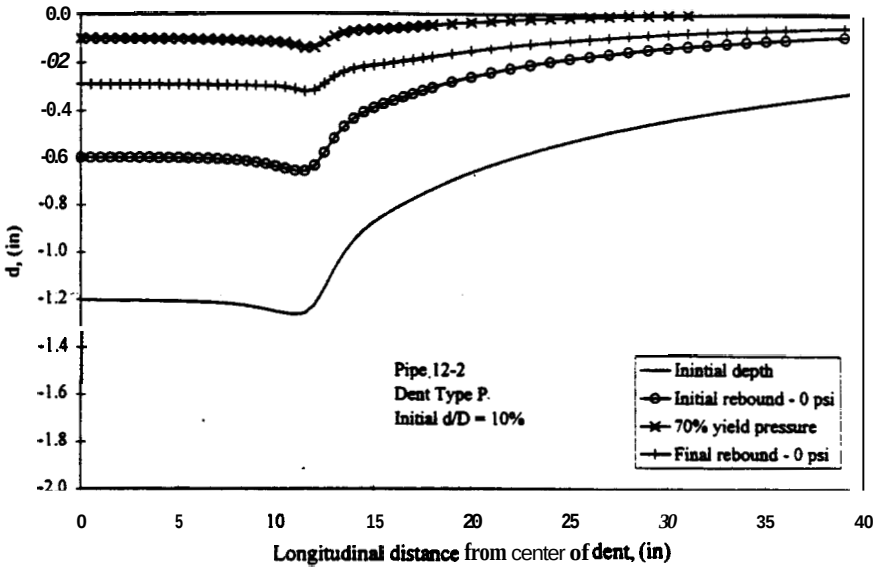

Figure 4-115: Type P dent shape history for a 10 percent *d/D* dent in Pipe 12-2.

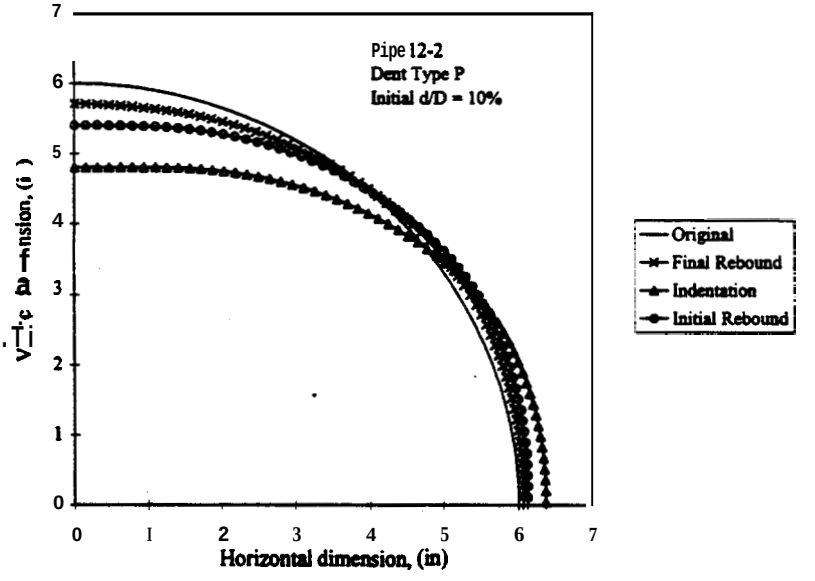

Figure 4-116: Dent Type P displaced cross section from indentation to final rebound for a 10 percent *d/D* dent in Pipe 12-2.

A graph of final d/D vs initial d/D for dent Type P is given in Fig. 4-117 for the pipes modeled. The large diameter 36 in. pipe has the most rebound. For-the 12 in. diameter pipes, an increase in wall thickness leads to a decrease in rebound. The relationship between initial and fmal depths is nearly linear for the different models. Thus, the averages of the Rebound Ratio for all dent depths gives fair approximations. The averaged values of the Rebound Ratio for Type P dents is given in Table 4-17.

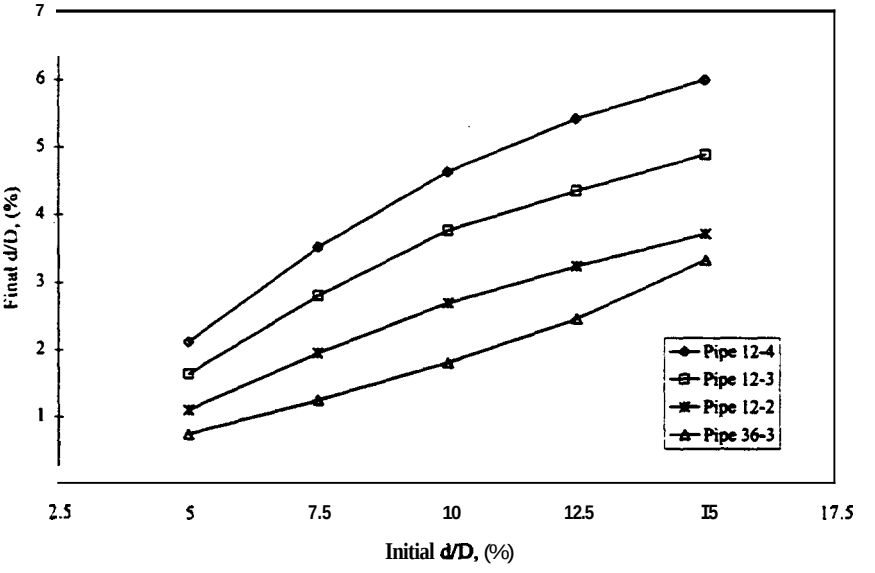

Figure 4-117: Final dent depth (d/D) vs. initial dent depth (d/D) for all Type P dents.

Table 4-17: Rebound Ratios for Type P dent.

Thickness, t (in.)	Diameter, D (in.)	
	12	36
0.250	0.25	-----
0.375	0.35	0.18
0.500	0.44	-----

The stress behavior of Type P dents is classified as long dent behavior. The flexible rebound characteristics of Type P dents makes the entire contact region susceptible to longitudinal fatigue crack development. An outside surface transverse stress contour plot of a 5 percent *d/D* Type P dent in Pipe 12-3 at the design pressure is given in Fig. 4-118. The region of high tensile stress extends fiom the periphery of the dent through the entire contact length longitudinally.

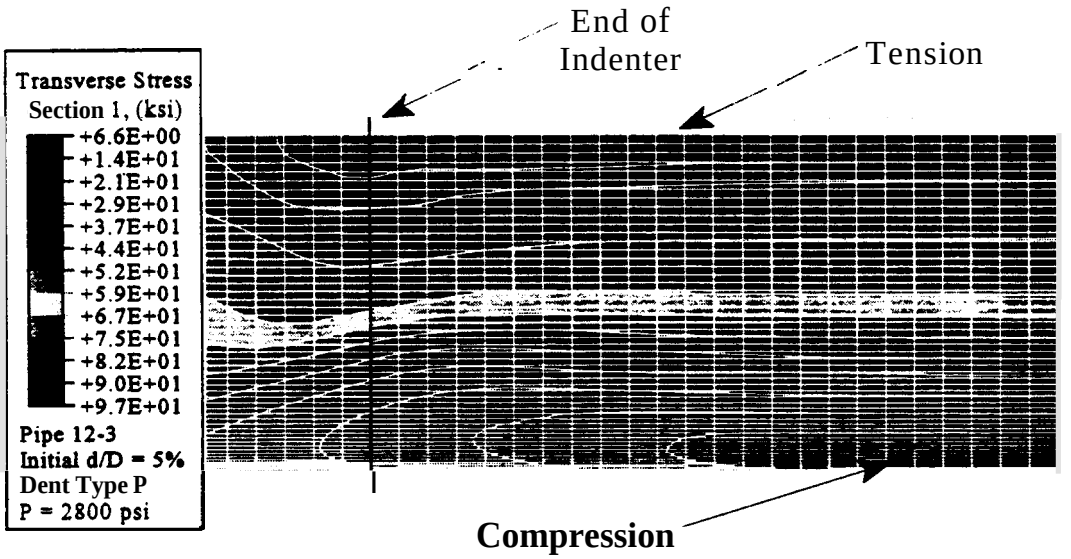

Figure 4-118: Outside surface transverse stress contour plot for Pipe 12-3 with a 5 percent *d/D* Type P dent at the design pressure.

All Type P dents have similar transverse stress distributions. An example is given for Pipe 12-2 with a 10 percent *d/D* Type P dent in Fig. 4-119. The entire dented region, including the dent periphery has a high stress range during pressure cycling. The stress range increases with increasing dent depth. The deeper dents have higher residual compressive stresses at zero pressure. The stress value at the design pressure remains above yield regardless of dent depth.

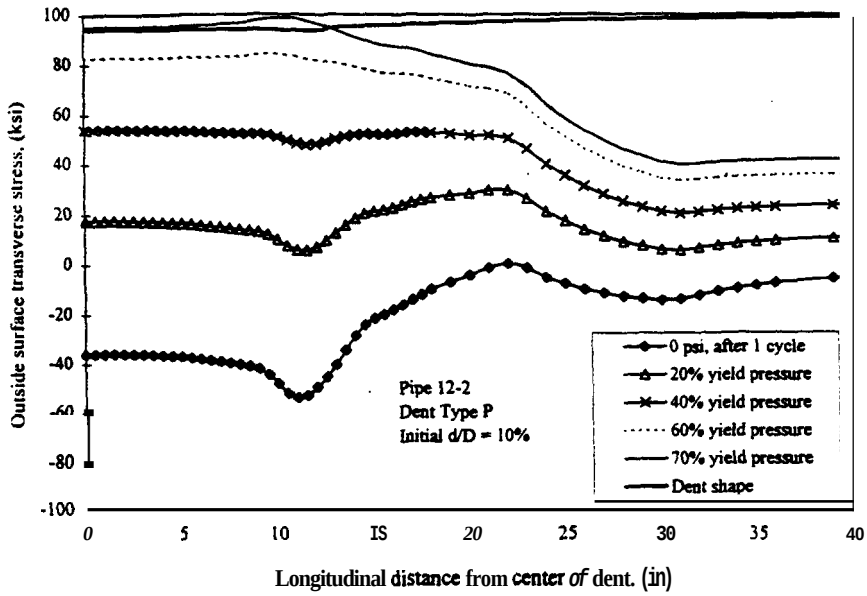

Figure 4-119: Outside surface transverse stress behavior during pressure cycling for Pipe 12-2 with a 10 percent *d/D* Type P dent.

4.7 RESTRAINED DENTS

4.7.1 Introduction

Restrained dents were tested in the experimental program for dent Types A, BH, and R, where R represents dents created by rocks. The method of restraint is given in Fig. 3-34 for a Type R dent. Industrial tie-down straps were used to prevent dent rebound by restraining the indenters. Two failure modes were found in the experimental testing of restrained dents. The most common mode of failure is identical to failure Mode 2 found for unrestrained longitudinal dents. This failure mode was found for all restrained dent types in the experimental program. The other mode of failure found for restrained dents involved the formation of transverse fatigue cracks with crack initiation of the inside pipe surface directly under the contact region of restrained rocks. This failure mode was not found for restrained Type A or BH dents.

Restrained dents were modeled using indenter Types A, BH, G, S1, and S8. Spherical indenters Types S1 and S8, were used to model the behavior of restrained rock dents (Type R) from the experimental program. Rocks without spherical contact regions gradually became spherical in shape with pressure cycling. High contact stresses are found at the ends of the contact region, as shown at the ends of the contact region for a Type A dent in Fig. 3-12. This causes high bearing stresses to degrade rocks around the edges of the contact region, gradually rounding the rock toward a spherical shape.

Two simple methods of restraint were used to model restrained dents. In the first case, the restraint remained rigid by forcing zero displacement of the restraint. In the other case, the restraining force remained constant throughout pressure cycling allowing rebound during cycling. The two cases are illustrated in Fig. 4-120. The two cases represent upper and lower bounds of restraint flexibility. The first case represents a rigid restraint with no flexibility. All restrained or settlement induced dents have some degree of flexibility. The second case represents a very flexible restraint. It allows rebound without a change in restraint force. The behavior of actual restrained dents would be bounded by these two cases.

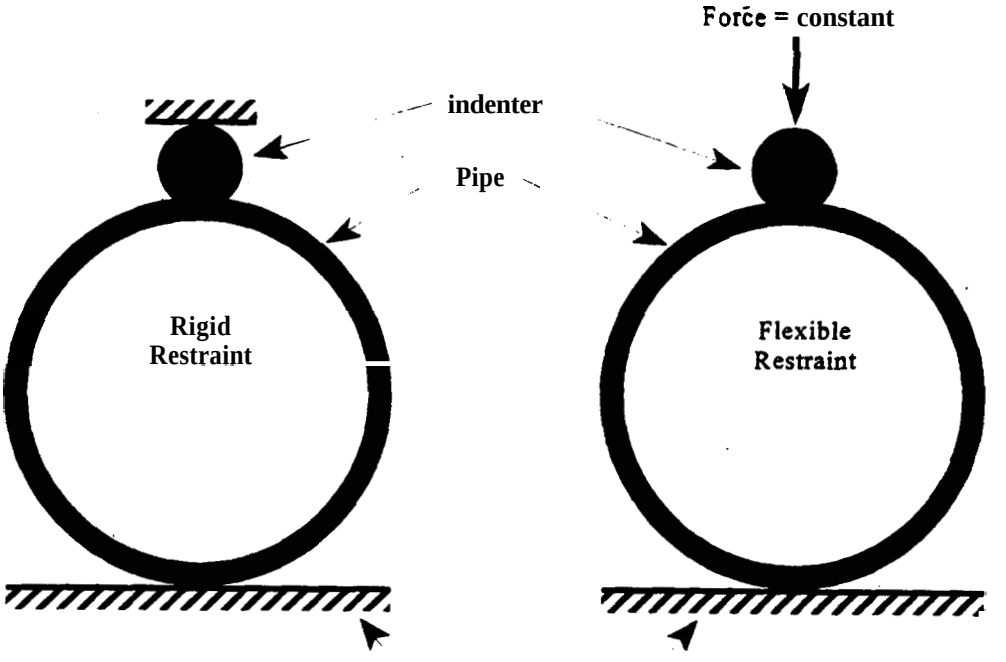

Figure 4-120: Methods of dent restraint modeled.

4.7.2 Peripheral Failures

Restraint of dents prevents rebound of dents. Peripheral fatigue cracks with outside surface crack initiation for restrained dents can occur similar to the behavior of short unrestrained dents representing failure Mode 2. All restrained dent types exhibit this behavior. Unrestrained Type A and G dents experience rebound which makes the dent contact region susceptible to failure Mode 1 with fatigue crack development in the dent contact region. By restraining these dents, rebound does not occur, which changes the failure mode from Mode 1 to Mode 2.

Type A and G restrained dents were modeled using the rigid restraint with zero displacement. The behavior of restrained dents with Mode 2 failures is similar regardless of the flexibility of the restraint for the two cases. For the models, indentation occurred with zero pressurization. Once the required dent depth was attained, pressure cycling began without

removal of the indenter. Pressurization causes additional plasticity of the dented region after indentation as the pipe deforms around the indenter shape. This is shown in Fig. 4-121. The curvature surrounding the contact region after indentation increases from pressurization.

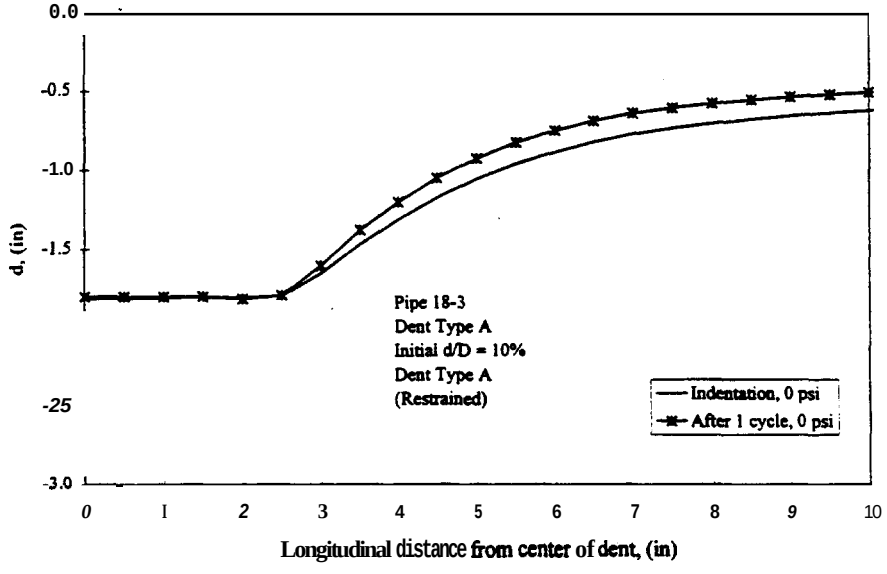

Figure 4-121: Restrained Type A dent depth at indentation and after pressure cycling for Pipe 18-3.

The outside surface transverse stress for the restrained 10 percent *d/D* Type A dent in Pipe 18-3 is given in Fig. 4-122. The transverse stress in the contact region remains in a state of compression through pressure cycling. The largest stress range is located in the dent periphery. This location with respect to the end of the contact region is similar to failure locations of unrestrained dents with Mode 2 failures. Similar stress behavior occurs for longer restrained dents. The outside Surface transverse stress for a restrained 10 percent *d/D* Type G dent in Pipe 18-3 is given in Fig. 4-123. As with the restrained Type A dent, the contact area is in compression and there is a high peripheral stress range for the restrained Type G dent.

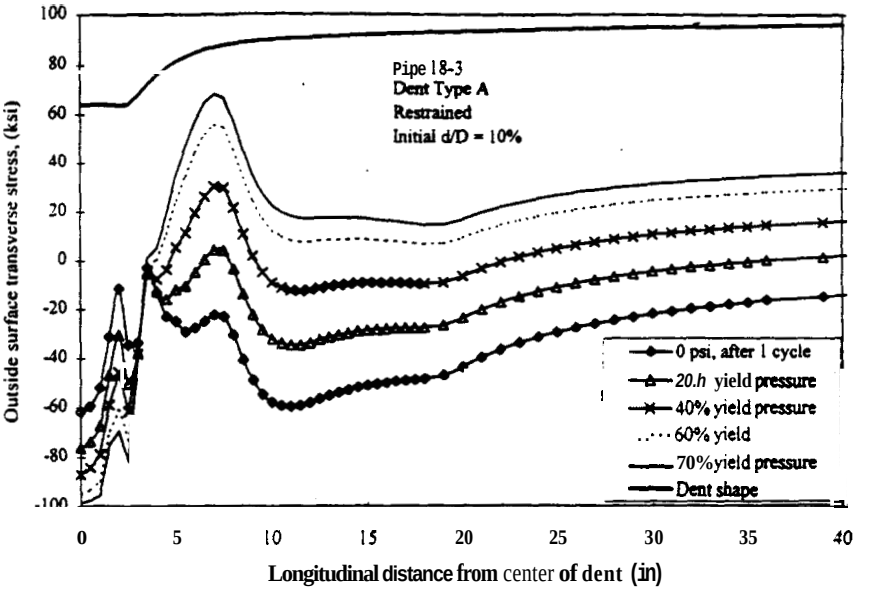

Figure 4-122: Outside surface transverse stress behavior during pressure cycling for Pipe 18-3 with a 10 percent *d/D* restrained Type A dent.

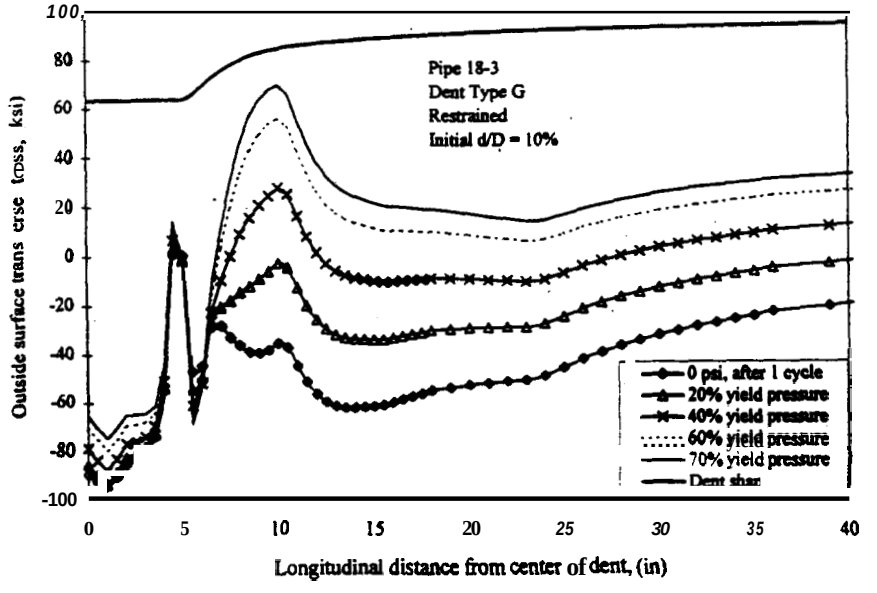

Figure 4-123: Outside surface transverse stress behavior during pressure cycling for Pipe 18-3 with a 10 percent *d/D* restrained Type G dent.

The restraining force is directly related to the internal pressure. Graphs of restraint force vs. pressure in terms of percent of yield pressure are given in Fig. 4-124 for restrained dent Types A and G. The restraining force for the longer Type G dent is higher than the force for the Type A dent due to the increase in dent length.

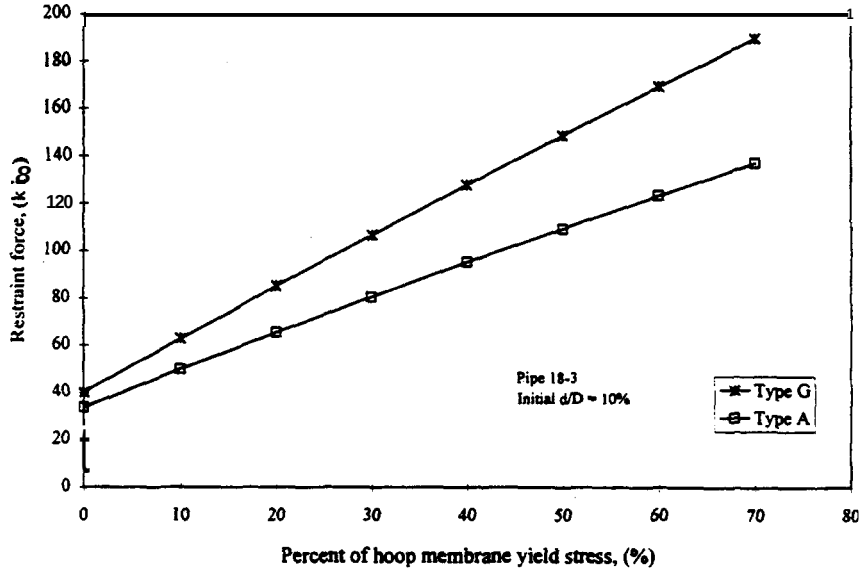

Figure 4-124: Restraint force vs. pressure for restrained Dent Types A and G.

Restrained spherical dents have outside surface transverse stress distributions indicative of Mode 2 failure with high tensile peripheral stress. A transverse stress contour plot of the outside surface for a 5 percent *d/D* restrained Type S1 dent in Pipe 18-2 at the design pressure is given in Fig. 4-125. The contact region remains in compression. High tensile stress is located in the entire periphery of the dent. Contour plots for other restrained dent types are similar to the one in Fig. 4-125.

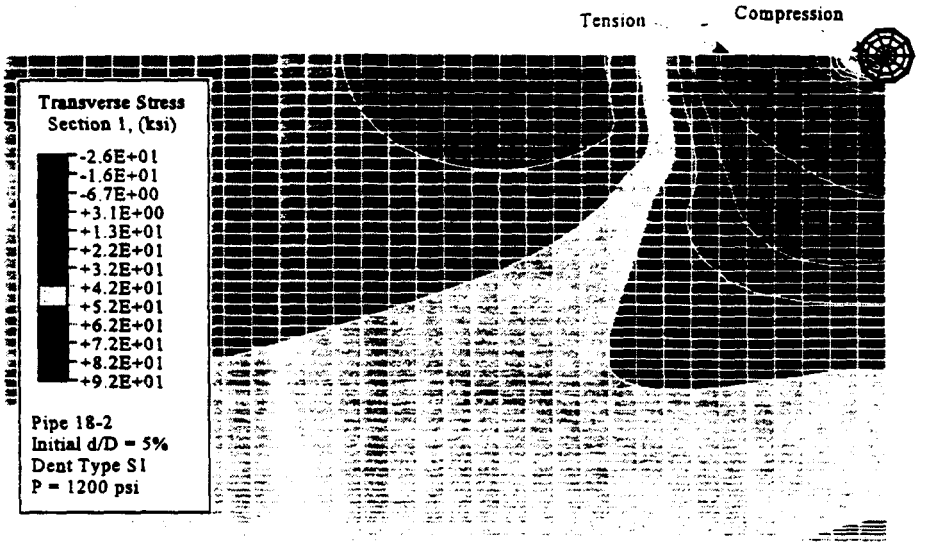

Figure 4-125: Outside surface transverse stress contour plot for Pipe 18-2 with a 5 percent *d/D* restrained Type S1 Dent at the design pressure.

4.73 Inside Surface Cracking Under Restrained Rocks

Restrained spherical dents were modeled to understand the cause of inside surface cracking found in the contact region of restrained rock dents (Type R) in the experimental program. Three fatigue cracks developed on the inside surface of restrained rock dents, oriented transverse to the longitudinal stress on Specimen 8 of the experimental program. Several specimens were tested with restrained rocks, but internal cracks only formed on Specimen 8. This pipe had a diameter of 18 in. and a wall thickness of 114 in. The three failures are summarized in Table 4-18. Initially, Dent 8-G failed at 61,295 cycles (Δp_{eff} = 435 psi.) and Dent 8-E failed at 68,264 cycles. Upon completion of the pressure cycling, a final static proof test was conducted to 77 percent of the yield pressure. This caused a periphery crack to leak at Dent 8-F. With the completion of the testing, all dented regions were removed from the specimen. Upon examination of the inside surface of Dent 8-F, the third internal surface crack was found. All three cracks were located directly under the contact region of the rocks. All three cracks propagated in the transverse direction of the pipe (normal to the longitudinal stress), unlike all

outside surface cracks, which were longitudinal.

Table 4-18: *Summary* of fatigue crack failures for Specimen 8 from experimental program.

Dent	*d/D* (%)	d (in.)	Cycles to Failure	Leak Location
8-E	**8.7**	**1.57**	68,264	internal crack under rock
8-F	**8.7**	1.57	**101,587**	external peripheral crack
8-G	6.8	**1.23**	61,295	internal crack under rock

The pressure histogram used for Specimen 8 had a low base pressure of 100 psi with maximum peaks ranging from 200 psi to 800 psi. The other specimens tested with rock dents were tested with a high base pressure which is more representative of actual pipeline pressures. The effective stress range of Specimen 8 is similar to the specimens tested with the high base pressure, but it has all cycles going to a low base pressure which does not represent typical pipeline pressures. This change in base pressure influenced the behavior of restrained rocks, relative to the other specimens.

The inside surface under the contact region of a rock maintains high tensile bending stress from indentation. Since the rock is restrained, no rebound occurs and the tensile stress remains on the inside d a c e . Upon pressurization, slight rebound of the dent occurs since the restraint was not perfectly rigid. This reduces the tensile bending stress on the inside surface. When the pressure is reduced, the rebound is recovered which increases the tensile bending stress. The formation of fatigue cracks is developed in the area of high tensile bending stress due to low pressure cycling. This suggests that this mode of fatigue crack development is less susceptible in pipes with high pressure cycling which keeps the inside surface at a lower state of tensile bending stress. No *fatigue* cracks developed in specimens tested with a high base pressure.

To better understand the behavior of restrained rocks, several finite element models were studied. The geometry of rocks is difficult to model due to variations in rock surfaces.

Settlement induced rock restraints can be of any shape and size. During settlement and pipe pressurization, rocks crack near the contact region(s) due to high bearing stresses. This resulted in a gradual rounding of the rock contact profile. However, due to the confinement of the dent shape and restraining force, cracked rocks usually maintain their general shape and dent depth. Spherical Type S1 and S8 restraints were selected to examine the general behavior of restrained rock dents.

As found in the experimental testing of Specimen 8, two types of fatigue failures can occur. Peripheral fatigue cracks with outside surface crack initiation can occur similar to the behavior of short unrestrained dents. Inside surface cracking can also develop under the dent contact region of rocks. All cracks of this type (internal) in the experimental program were transverse in direction. The behavior of the contact region of restrained dents is influenced by restraint geometry and stiffhess, which affect the inside surface stress distributions.

Spherical Type S1 and S8 restraints were modeled on Pipes 18-2 and 48-3. Both methods of restraint consisting of the rigid and flexible cases as shown in Fig. 4-120 were modeled to study the internal cracks. The formation of internal transverse fatigue cracks is directly related to the inside surface longitudinal stress range. The inside surface longitudinal stress is influenced by the dent shape, dent depth, and restraint flexibility. Figure 4-126 shows the inside surface longitudinal stress behavior of a Type S1 flexible restraint in Pipe 18-2. The restraining force was set equal to the denting force for this model. The flexibility of the restraint allows rebound. The smallest dent has the highest stress range of all dents. The stress level of all dent depths is above yield at zero pressure. The deep dents have high tensile stress at all pressures. These dents have a high state of stress, but have a low stress range. For this specific case, the shallow dent has the lowest fatigue life for internal transverse cracks. The deep dents may be more susceptible to another type of failure such as periphery cracks. Stress contour plots for the 5 percent d/D dent in Fig. 4-126 are given in Figs. 4-127 and 4-128. Figure 4-127 gives the inside surface longitudinal stress at zero pressure after one cycle. Note that the inside longitudinal stress at the dent contact region is in high tension. Figure 4-128 shows the inside surface longitudinal stress at the design pressure. The stress at the dent contact region is small.

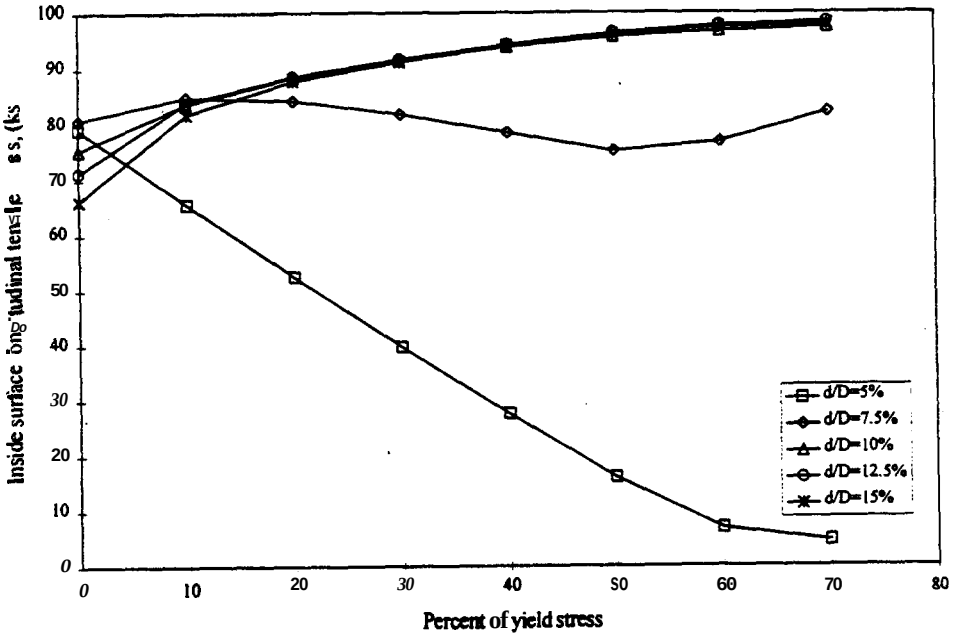

Figure 4-126: Inside surface longitudinal stress distribution of Pipe 18-2 with a restrained Type S1 dent with a flexible restraint.

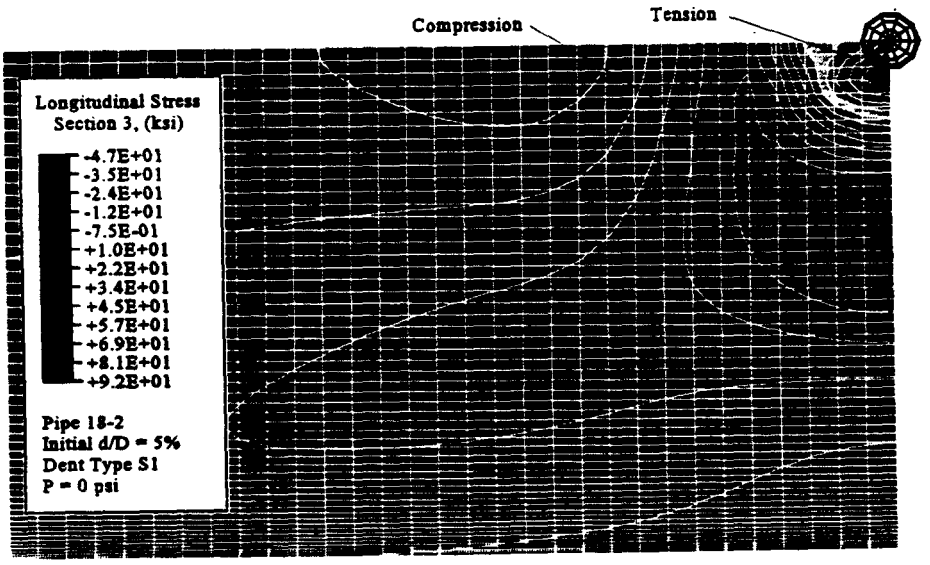

Figure 4-127: Inside surface longitudinal stress contour plot for Pipe 18-2 with a restrained Type S1 dent with a flexible restraint at zero pressure.

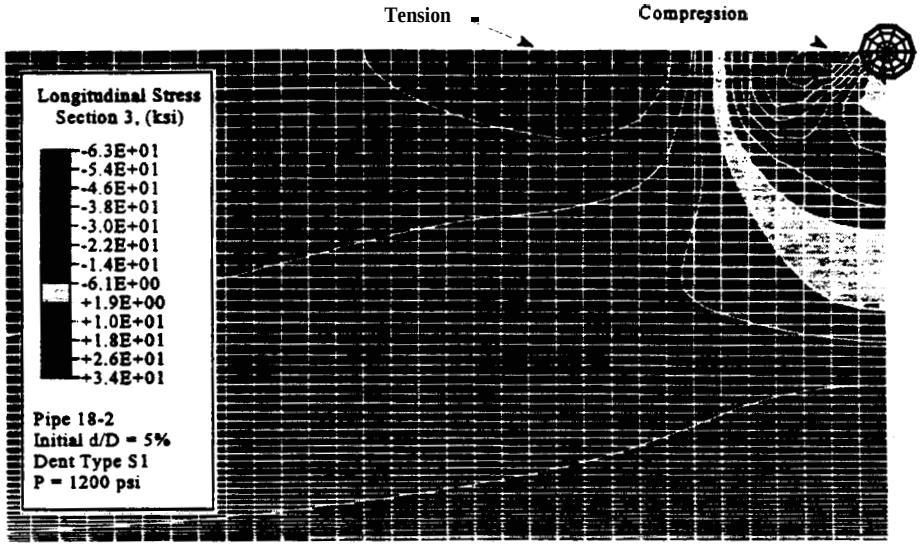

Figure 4-128: Inside surface longitudinal stress contour plot for Pipe 18-2 with a restrained Type S1 dent with a flexible restraint at the design pressure.

The influence of dent shape is given by comparing Figs. 4-126 and 4-129. The model of Fig. 4-129 is identical to that of Fig. 4-126 except that the spherical restraint diameter is 8 in. instead of 1 in. For the larger diameter restraint, the stress range increases for the deeper dents. The shallowest dent still has the highest stress range for the larger restraint. The larger diameter restraint makes a wider range of dent depths susceptible to internal transverse cracks. This is also shown in Figs. 4-130 and 4-131. Figure 4-130 shows the internal longitudinal stress of the 1 in. spherical restraint on pipe 48-3. Figure 4-131 shows the stress of the 8 in. restraint on pipe 48-3. Figure 4-130 has similar stress distributions as Fig. 4-126 where only the shallow dent has a high stress range, and the deeper dents maintain a high state of stress with a low stress range. In Fig. 4-131, the stress range is highest for the shallowest dent as in Fig. 4-130. The deeper dents have higher stress ranges than those is Fig. 4-130, but the stress range is most likely not large enough to initiate cracking. Failures will most likely occur from peripheral cracking for the deeper dents.

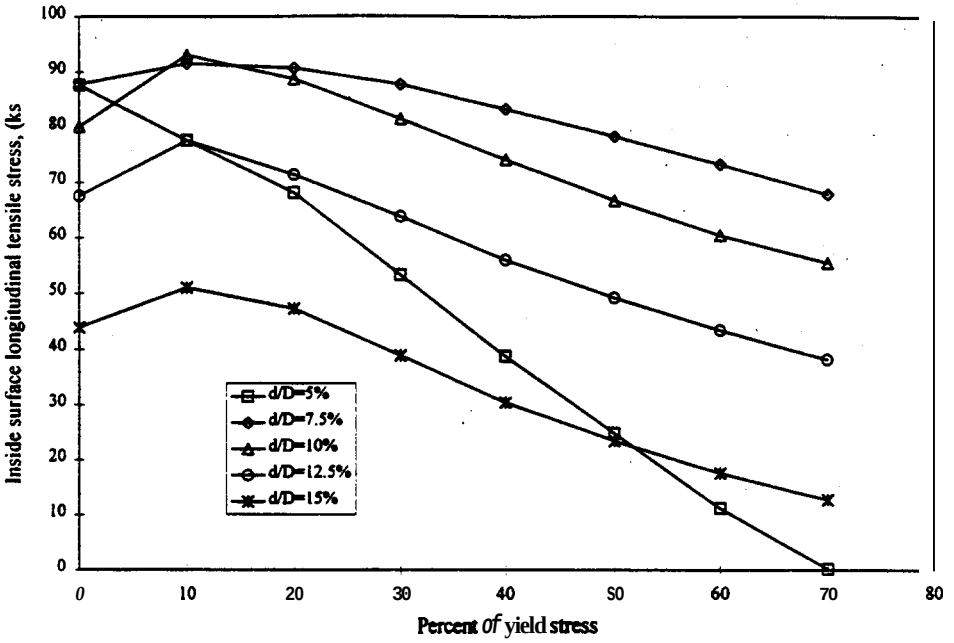

Figure 4-129: Inside surface longitudinal stress distribution of Pipe 18-2 with a restrained Type S8 dent with a flexible restraint.

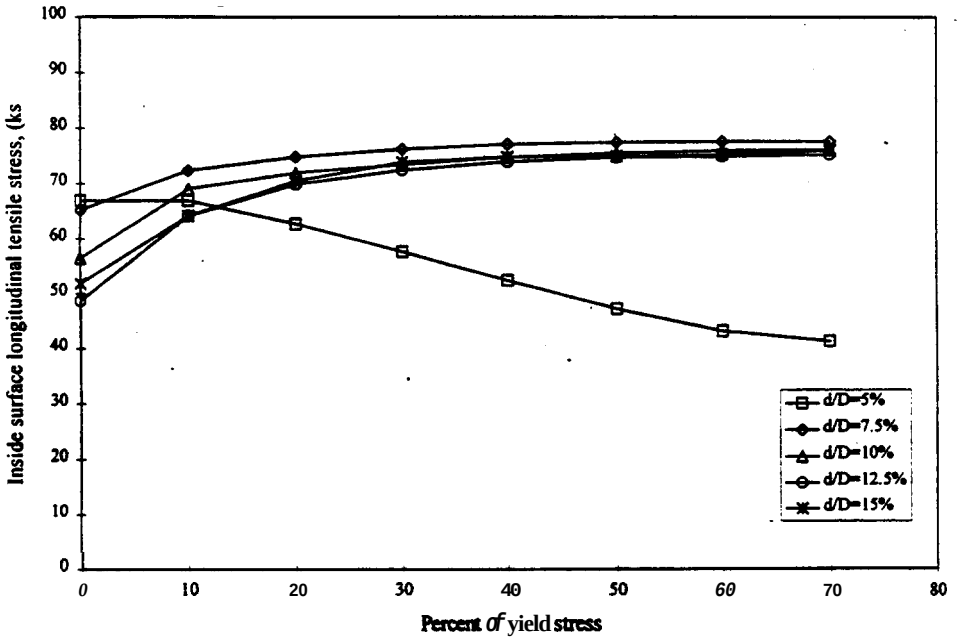

Figure 4-130: Inside Surface longitudinal stress distribution of Pipe 48-3 with a restrained Type S1 dent with a flexible restraint.

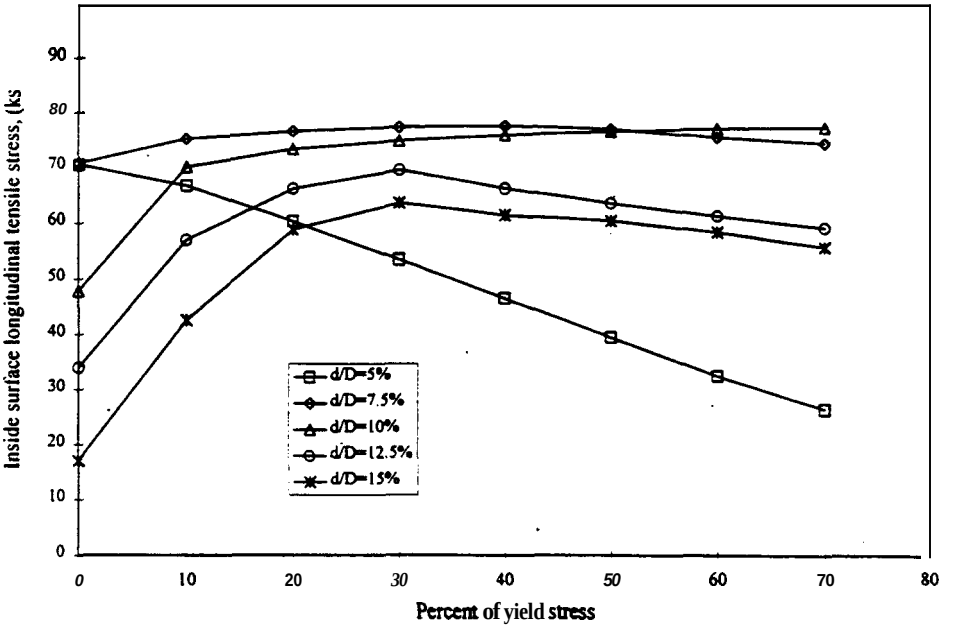

Figure 4-131: Inside surface longitudinal stress distribution of Pipe 48-3 with a restrained Type S8 dent with a flexible restraint.

The restraint initially puts all dents in a high state of tensile bending stress on the inside surface of the dent contact region. Upon pressurization, the pipe forms around the restraint, which increases the bending stress. After the pressure is removed, the tensile bending stress decreases due to elastic rebound as the curvature of the dent contact region decreases. This behavior is only influenced by the change in curvature of the dent contact region caused by pressure change.

The inside surface bending stress is also influenced by the restraint rebound behavior. A flexible restrained dent rebounds with pressure. The reduction in dent depth decreases the curvature of the dent around the restraint. This implies that with flexible restraints, the inside surface bending stress decreases with dent rebound caused by increasing pressure.

The effect of pressure of the change is curvature is given in Fig. 4-132, which shows the inside surface longitudinal stress distribution of Pipe 18-2 with a rigid Type S8 restraint. During

indentation and pressurization of the first cycle, the inside surface is in a state of high tensile stress due to the curvature from indentation and pressurization. When the pressure was removed from the first cycle, the curvature decreases. This causes the inside surface longitudinal bending stress to decrease. After the initial cycle, the stress increases with pressure due to the increase in curvature.

The stress distributions of Fig. 4-132 represent a rigid restraint. If rebound is allowed for the same restraint as given in Fig. 4-129, the stress distribution changes dramatically. The curvature change due to rebound is more significant than that caused by the formation of the contact surface around the restraint. With the flexible restraint, the inside surface stress at zero pressure is higher with increasing dent flexibility. Upon pressurization of the flexible restraint, rebound causes the decrease in curvature which reduces the inside surface stress.

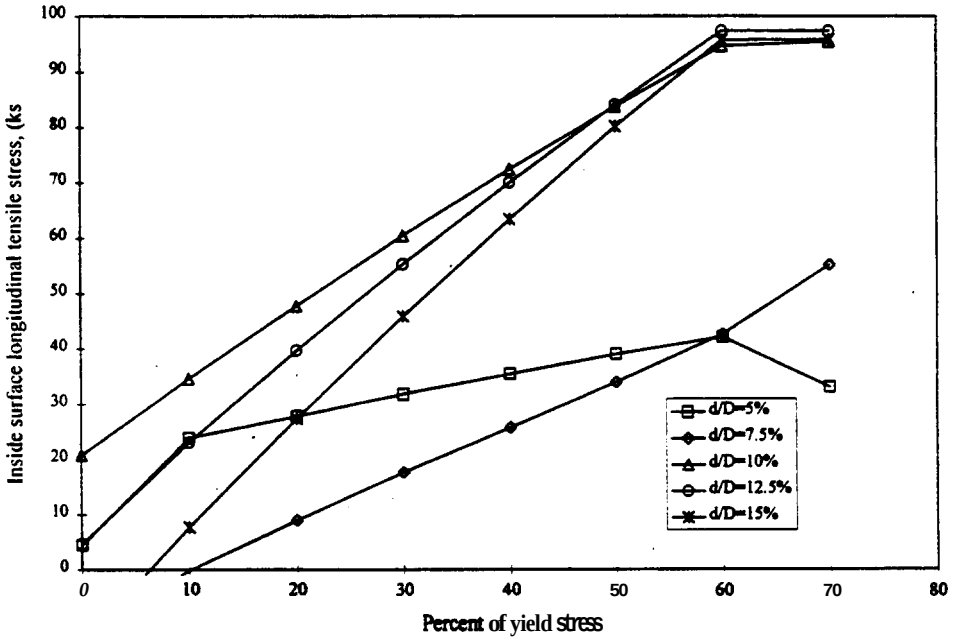

Figure 4-132: Inside d a c e longitudinal stress distribution of Pipe 18-2 with a restrained Type S8 dent with a rigid restraint.

The fatigue behavior of the dent contact region of restrained dents is influenced by dent depth, restraint flexibility, and dent shape. Deeper dents have more curvature of the dent contact region causing higher tensile stress distributions with lower stress ranges. Shallower restrained

dents are more susceptible to internal cracking due to the increased stress range. The restraint flexibility influences the stress behavior of restrained dents. Rigid restraints give inside surface stress distributions that increase with increasing pressure. Flexible restraints have inverse stress distributions. The flexibility of restraints is difficult to predict. The dent size has little influence of the stress behavior for the spherical restraints. Smaller restraints are less susceptible to inside surface cracking for deep dents. The stress range of deep dents with larger restraints is higher. The difference in pipes has little influence for the pipe sizes modeled.

4.8 MISCELLANEOUS PARAMETERS

4.8.1 Longitudinal Stress

The longitudinal membrane stress was varied fiom 30 to 50 percent of the hoop membrane stress. The models for all dent types studied were given a longitudinal stress of 50 percent of the hoop stress. This amount of longitudinal stress represents a pressure vessel, not a buried pipeline. Longitudinal stress in buried pipelines can be reduced fiom 50 percent found in pressure vessels to approximately 30 percent of the hoop stress due to longitudinal expansion and soil skin friction. A model was analyzed using a longitudinal stress of 30 percent of the hoop stress to make comparisons with the longitudinal stress of 50 percent used in the models.

The longitudinal stress was varied for Pipe 24-3 with Type A dents modeled as grade X60. Little difference in behavior of the dent was found between the two different values of longitudinal stress. The model with a longitudinal stress of 50 percent of the hoop stress had slightly more rebound than the longitudinal stress of 30 percent as shown in Table 4-19. Thus, the rebound characteristics of dents are not significantly influenced by longitudinal stress

Fatigue cracks initiate in the longitudinal orientation from transverse stress in the dented region for unrestrained dents. The longitudinal membrane stress has little influence on the transverse stress. Transverse stress distributions are similar for models with longitudinal stress set to 30 or 50 percent of the hoop stress. Thus, the longitudinal stress does not influence the fatigue behavior of unrestrained dents in pipelines.

Table 4-19: Final dent depth (d/D) for different longitudinal stresses for Pipe 24-3 with Type A dents.

Initial d/D (%)	Longitudinal Membrane Stress as Percentage of Hoop Stress	
	50%	30%
5.0	0.35	0.35
7.5	0.55	0.55
10.0	0.69	0.70
12.5	0.78	0.79
15.0	0.84	0.87

4.8.2 Pipe Grade and Pressure History

Three different pipe grades were modeled. They include API grades B (35 ksi), X42 (42 ksi), and X60 (60 ksi) as discussed in Sec. 4.2.2. The change in rebound and stress behavior due to changes of pipe grade and pressure history were studied. The pressure histories supplied for the models is based on percentage of the yield pressure as discussed in Sec. 4.3.2. For a given pipe and dent combination, six sets of models were analyzed with different pipe grades and pressure histories. The pressure histories were all based on the three pipe grades. The six combinations of pipe grades and pressure histories is given in Table 4-20. The six combinations were modeled for unrestrained longitudinal dent Types A and BH on Pipes 24-2 and 30-3. The design pressures for the various grades modeled for the two pipes is given in Table 4-21. Several comparisons can be made for rebound and stress behavior from the six combinations.

Table 4-20: Pipe grades and pressure histories studied.

Model Set	Pipe Grade	Pressure history based on pipe grade
1	X60 (60 ksi)	X60 (60 ksi)
2	X60 (60 ksi)	X42 (42 ksi)
3	X60 (60 ksi)	B (35 ksi)
4	X42 (42 ksi)	X42 (42 ksi)
5	X42 (42 ksi)	B (35 ksi)
6	B (35 ksi)	B (35 ksi)

Table 4-21: Design pressures for Pipes 24-2 and 30-3.

Pipe	Grade	Design Pressure (psi)
24-2	X60	894
	X42	626
	B	521
30-3	X60	1077
	X42	754
	B	628

The rebound behavior of unrestrained dents is primarily influenced by pressure history and not pipe grade. Dent depth data presented in terms of the Rebound Ratio is given in Table 4-22 for dent Types A and BH in Pipes 24-2 and 30-3 for the pipe grade and pressure history model sets. The Rebound Ratio for the Type A dent in Pipe 24-2 modeled with a grade of X60 and a pressure history of X60 is 0.19. If the pressure history is reduced to that of grade B, resulting in a lower maximum pressure for the pipe, the Rebound Ratio is increased to 0.25.

Thus, a decrease in the maximum pressure causes an increase in the Rebound Ratio, which corresponds to a decrease in rebound. This behavior illustrates one of the problems with developing acceptance criteria of dents based solely on dent depth.

Table 4-22: Rebound Ratios for combinations of pipe grades and pressure histories.

Pipe	Dent	Pipe Grade	Pressure based on grade:		
			X60	X42	B
24-2	Type A	X60	0.19	0.23	0.25
		X42	-----	0.23	0.27
		B	-----	-----	0.26
24-2	Type BH	X60	0.29	0.35	0.37
		X42	-----	0.36	0.39
		B	-----	------	0.38
30-3	Type A	X60	0.22	0.32	0.36
		X42	-----	0.32	0.38
		B	----	---	0.40
30-3	Type BH	X60	0.36	0.42	0.44
		X42	-----	0.43	0.46
		B	-----	-----	0.49

At the time of detection of a dent, rebound will have probably occurred from pressurization. Determination of the initial dent depth can be used to estimate a damage term for fatigue strength. The maximum pressure in the pipe after indentation and before detection must be estimated to determine what Rebound Ratio should be used to estimate the initial dent depth. The estimation of the maximum pressure prior to detection should be overestimated for determining what Rebound Ratio to use. This will cause a conservatively large estimation of the initial dent depth.

The grade of the pipe has little influence on the rebound behavior of dents. For pipes of different grades with identical pressure histories, the Rebound Ratios are very similar. Pipe grades of X60 and B in Pipe 24-2 with Type A dents with pressure histories based on grade B have Rebound Ratios of 0.25 and 0.26, respectively. The rebound behavior involves significant plastic flow regardless of the yield strength. The pipe *grade* only influences the design pressure. Thus, pipes with higher grades have higher design pressures leading to an increase in rebound directly caused by an increase in the pressure history, not caused by the yield strength.

The increase in rebound based on higher design pressures is easily noticed in the graphs of Rebound Ratios such as in Fig. 4-55 for Type A dents. In the figure, diameters up to 24 in. were modeled with grade X60 with a pressure history based on the design pressure for a specified minimum strength of 60 ksi. Diameters of 30 in. and above were modeled with grade B with a pressure history based on the design pressure for a specified minimum yield strength of 35 ksi. The smaller diameter pipes experience more rebound from an increase in the design membrane hoop stress or pressure.

The pressure *history* influences the stress behavior of dents. Higher pressure histones will likely reduce the fatigue life of a dent. The pressure history *can* also influence the failure mode of dents. For longitudinal Type A dents, an increase in the maximum pressure after indentation will increase rebound potentially causing the failure mode to shift from Mode 2 with peripheral cracking to Mode 1 with cracks developing in the damaged contact region. A shift in failure mode caused by the increase in maximum pressure can severely reduce the fatigue strength of a dent.

The outside d a c e transverse stress distribution of a 15 percent *d/D* Type A dent in Pipe 30-3 with a grade of X60 and a pressure history based on grade X60 is given in Fig. 4-133. The high stress range is located in the center of the dent indicative of failure Mode 1 with fatigue crack development in the dent contact region. The stress distribution of the Same dent with a pipe *grade* of B and a pressure history of grade B is given in Fig. 472. For this model with a lower maximum pressure based on pipe grade B, the stress range is indicative of a Mode 2 failure

with peripheral fatigue crack development. Comparing the two pressure histories shows how the maximum pressure after indentation can influence the stress distribution during pressure cycling. For the Type A dent in Pipe 30-2, the fatigue life of the dent with the higher maximum pressure with predicted failure Mode 1 will be considerably lower than the dent with the lower maximum pressure with predicted failure Mode 2.

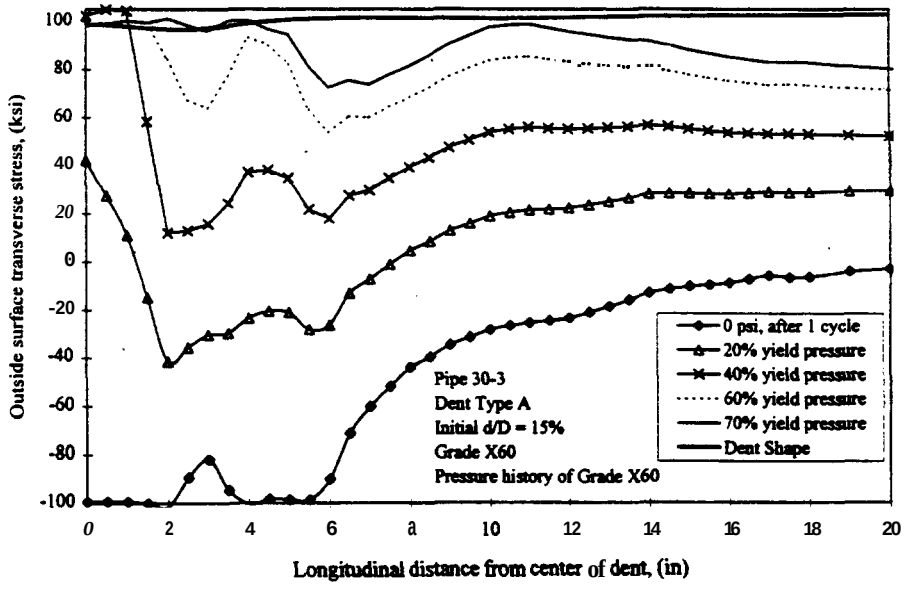

Figure 4-133: Outside surface transverse stress behavior during pressure cycling for Pipe 30-3 with a 15 percent *d/D* Type A dent with a grade of X60 and a pressure history based on Grade X60.

Regardless of the failure mode, an increase in the maximum pressure will reduce the fatigue strength of a dent. Additional pressurization will cause an increase in rebound. The increase in plastic flow of the dented region from the increase in rebound will accelerate crack initiation.

4.83 Support Conditions During Indentation

Support conditions of the pipe were studied during the step of indentation. Two support conditions were modeled. Pictures of the support conditions modeled is given in Fig. 4-4. The first support condition is flexible allowing deflection of the circular cross section of the pipe. The second support modeled is rigid not allowing deflection of the circular cross section. Actual support conditions will be bounded by these two cases. Influence of support conditions are studied for indentation forces, rebound behavior, and stress behavior.

The amount of rebound that occurs in a dent is related to the support conditions at indentation. The cross section displaced shape during indentation of Pipe 18-2 with a Type A dent using the flexible support condition is given in Fig. 4-134. The corresponding displaced shape for the rigid support is given in Fig. 4-135. The flexible support allows the cross section to displace to an elliptical shape. The rigid support does not allow this, causing more localized deformation in the dented region. The stiffness provided to resist global deflection to an elliptical shape requires higher indenter forces to develop dents of equal depth for the two support conditions.

The indenter forces required for dent formation are influenced by dent depth and support conditions. For the models studied, a graph of indenter force vs. dent depth is given in Fig. 4-136 for the two support conditions. In general, the indenter forces for dents with the flexible support are approximately 60 percent of the forces with the rigid support. The increase of indenter force with increasing support rigidity causes an increase in deformation of the indenter contact area.

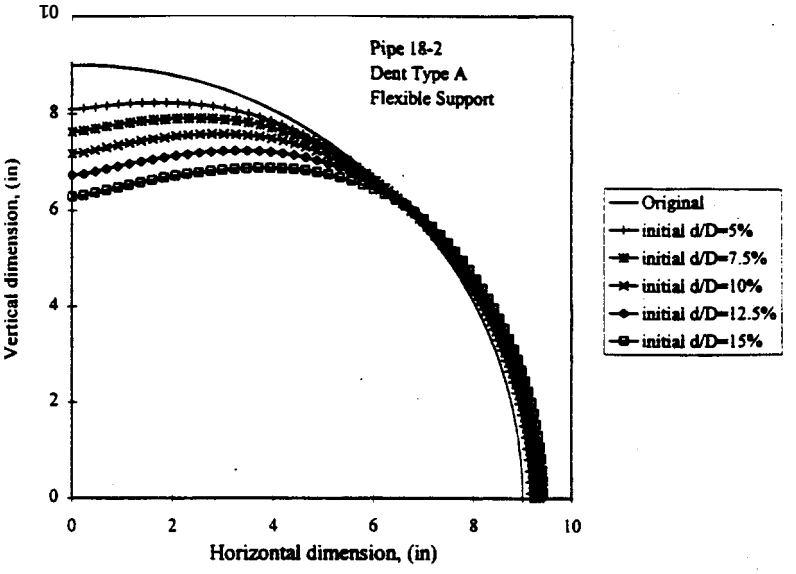

Figure 4-134: Displaced cross section at indentation with the flexible support condition.

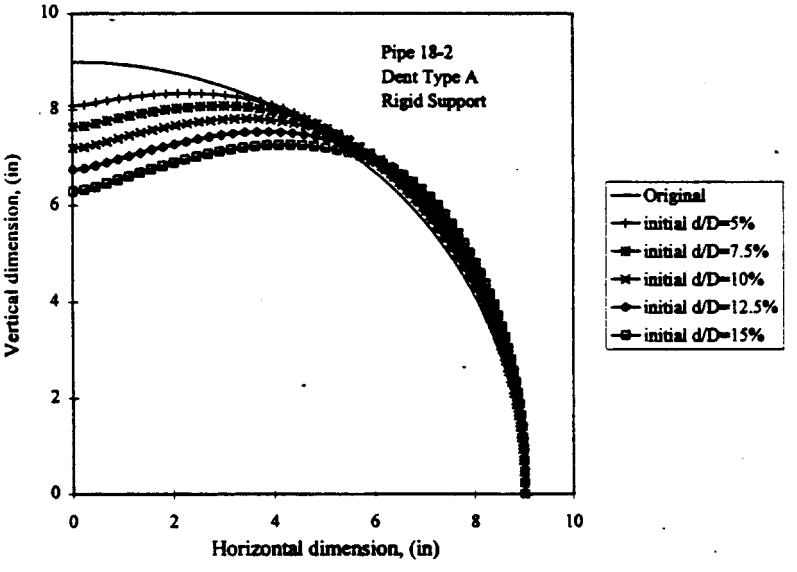

Figure 4-135: Displaced cross section at indentation with the rigid support condition.

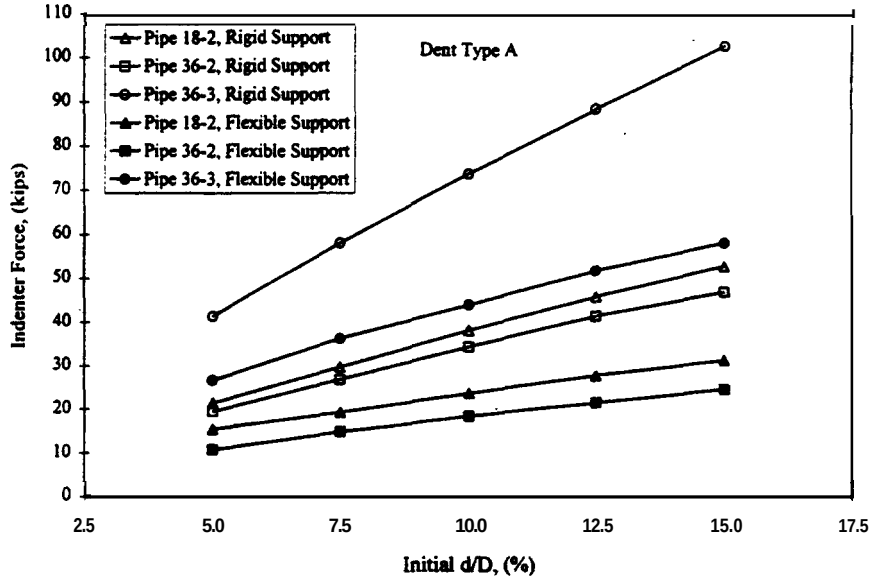

Figure 4-136: Indenter force vs. dent depth for flexible and rigid support conditions.

Dents with the flexible support condition rebound more than dents with the rigid support condition. The flexible support allows the global deflection which is almost entirely recovered during rebound. The rigid support causes higher localized deformation which has less rebound. For the models studied, a graph of final dent depth (d/D) vs. initial dent depth (d/D) is given in Fig. 4-137 for the two support conditions. The final dent depths for the dents with the flexible support are approximately 65 percent of the final depths with the rigid support. Models for Pipe 18-2 experienced convergence difficulties for dent depths above 7.5 percent d/D for the rigid support condition.

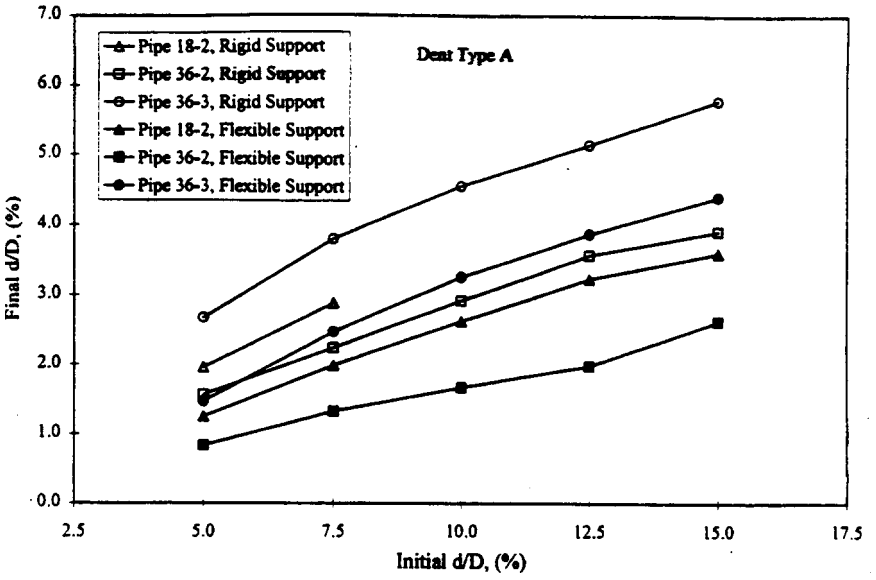

Figure 4-137: Final dent depth (d/D) vs. initial dent depth (d/D) for flexible and rigid support conditions.

The stress behavior is influenced by the support conditions at indentation. The influence can be related to the rebound behavior for the different support conditions. The outside surface transverse stress distribution for a 10 percent d/D Type A dent in Pipe 36-3 with the rigid support is given in Fig. 4-138. The stress distribution for the same initial dent depth with the flexible support is given in Fig. 4-139. Both distributions predict failure Mode 2. The stress range in the contact region is lower for the dent with the rigid support during indentation. The final dent depths for the 10 percent d/D Type A dents in Pipe 36-3 are 4.6 and 3.3 percent d/D for the rigid and flexible support conditions, respectively. The dent with the rigid support behaves like a dent with a flexible support of deeper initial dent depth. The stress distribution for the 10 percent d/D dent in Fig. 4-138 with the rigid support is very similar to the stress distribution for a 15 percent d/D dent with the flexible support, which is given in Fig. 4-140. The final dent depth of this dent is 4.4 percent d/D, which is slightly lower than that of the 10 percent d/D dent with the rigid support. The similarities of rebound and stress behavior of the 10 percent d/D dent with rigid support and the 15 percent d/D dent with flexible supports suggests that the dents with rigid support can be treated as dents with flexible support of deeper initial depth.

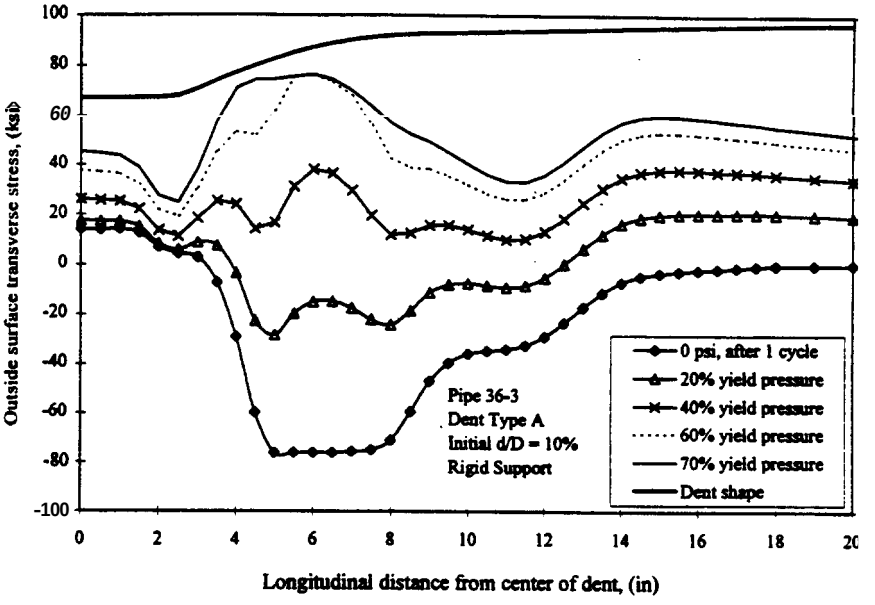

Figure 4-138: Transverse stress behavior during pressure cycling for Pipe 36-3 with a 10 percent *d/D* Type A dent with rigid support conditions.

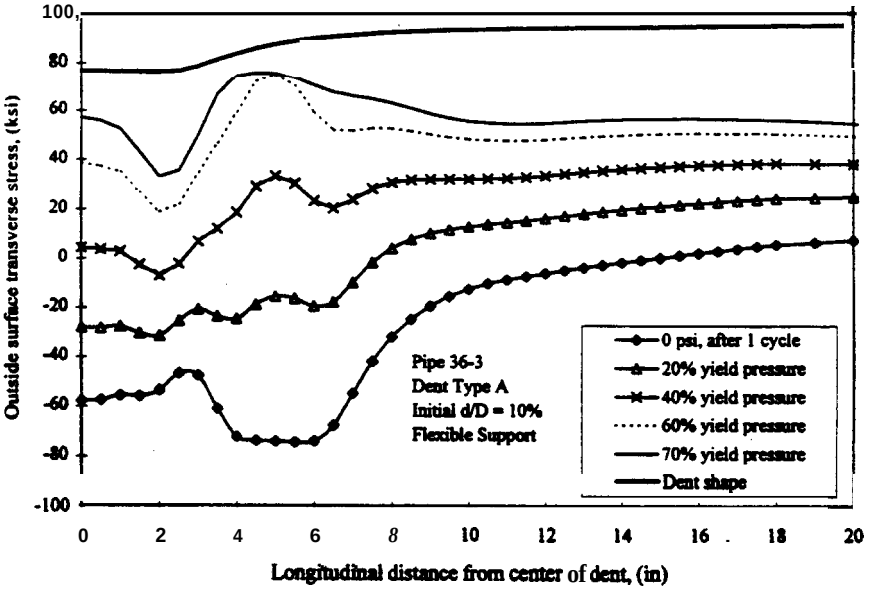

Figure 4-139: Transverse stress behavior during pressure cycling for Pipe 36-3 with a 10 percent *d/D* Type A Dent with flexible support conditions.

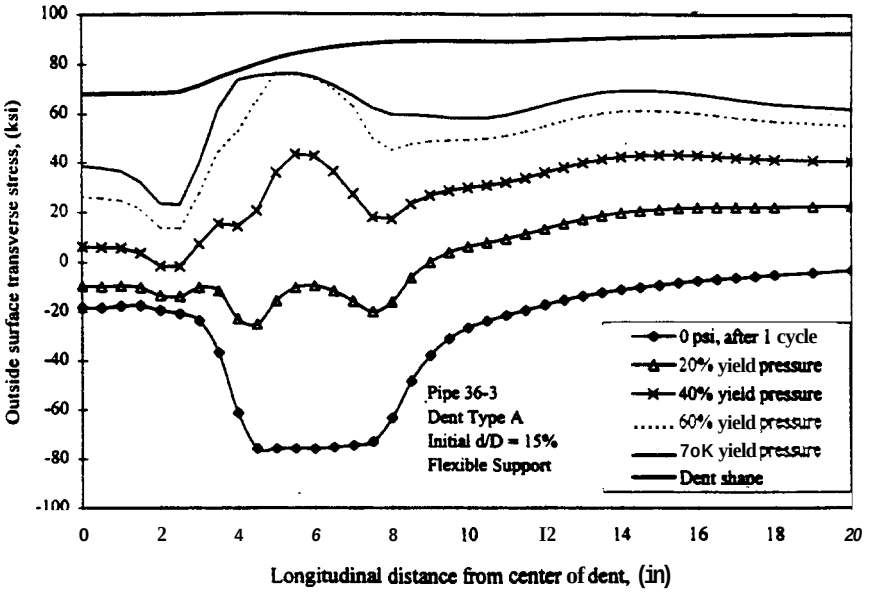

Figure 4-140: Transverse stress behavior during pressure cycling for Pipe 36-3 with a 15 percent *d/D* Type A Dent with flexible support conditions.

4.8.4 Pressure During Indentation

The dent formation process will most likely occur during service of the pipeline. Thus, indentation usually occurs with internal pressure in the pipe. All of the modeling performed involved indentation with zero internal pressure. Additional models of Pipe 18-2 were analyzed where internal pressure was present during indentation. The internal pressures used are based on percentage of the yield pressure, as with the pressure histories. Indentation was modeled with internal pressures of 0, 20, 40, and 70 percent of the yield pressure, which represent pressures of 0, 343, 686, and 1200 psi, respectively, for pipe grade X60. Convergence difficulties occurred for all of the models during pressure cycling for initial dent depths of 10 percent *d/D* and higher. Thus, there are limited results for deeper dents.

The indenter forces required to form dents is influenced by the internal pressure at indentation. A graph of indenter force vs. dent depth is given in Fig. 4-141 for the different

pressures modeled during indentation. An increase in pressure requires an increase in indenter force to create a dent of a certain depth. The required indenter forces increase by a factor of two by increasing the internal pressure from 0 psi to 20 percent of the yield pressure. The indenter forces with an internal pressure of 70 percent of the yield pressure are 3.75 times greater than the forces required at 0 psi. The indenter force required to create a 15 percent d/D Type A dent at the design pressure is 125 kips. This is an extremely high load to be applied normal to an 18 in. pipe with a thickness of only 0.25 in. In a pipeline, this large of a force will likely cause severe contact damage leading to rupture of the pipe during indentation, if it could be applied at all. A practical upper bound of the maximum applicable force during indentation in pipelines is likely lower than 125 kips.

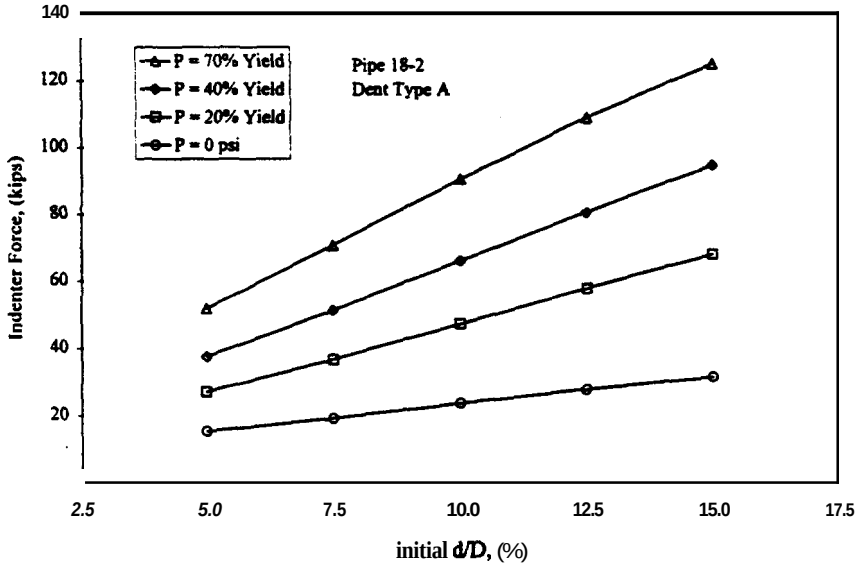

Figure 4-141: Indenter Force vs. Dent Depth for Different Internal Pressures during Indentation.

The internal pressure during indentation influences the rebound characteristics of dents. A graph of final d/D vs. initial d/D is given in Fig. 4-142 for Pipe 18-2 with Type A dents for the different pressures modeled during indentation. The largest increase in residual dent depth based on pressure at indentation is from zero internal pressure to 20 percent of the yield pressure. Further increases of the pressure during indentation yield higher final dent depths, but not

significantly larger than the depths for indentation at 20 percent of the yield pressure.

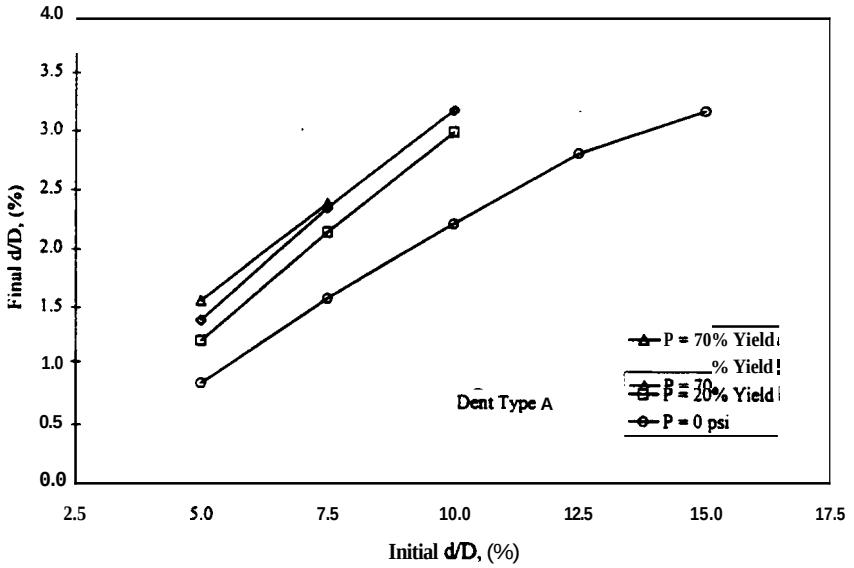

Figure 4-142: Final dent depth (d/D) vs. initial dent depth (d/D) for different internal pressures during Indentation.

The stress distributions during pressure cycling for dents which were formed under pressure are similar to dents formed with no internal pressure. Support conditions as discussed in Sec. 4.8.3 have more influence on the stress distribution than the pressure at indentation. The influence of pressure during indentation can be considered as part of the support conditions. Increasing pressure at indentation affects dent behavior similar to an increase of rigidity of support conditions, but to a lesser degree.

4.9 COMPARISONS OF MODELS WITH EXPERIMENTAL TEST SPECIMENS

4.9.1 Introduction

Comparisons between the finite element models and test specimens fiom the experimental program are made to verify the results fiom the models. Comparisons are made for rebound behavior and failure mode of unrestrained dents. Fifteen specimens were tested in the experimental program. They are given in Table 4-23 with pipe dimensions and pressure histories.

Table 4-23: *Summary* of test specimens in the experimental program.

Specimen No.	Diameter, D (in.)	Thickness, t (in.)	API 5L Grade	Pressure Cycling History			
				Base Press. (psi)	P_{min} (psi)	P_{max} (psi)	Effective ΔP (psi)
1	12.75	0.375	X60	100	100	1050	553
2	12.75	0.375	X60	100	100	1050	553
3	12.75	0.250	X42	100	100	1200	721
4	16	0.250	X60	100	100	800	435
5	16	0.250	X42	813	100	948	434
6	18	0.250	X42	720	100	840	383
7	18	0.250	X60	100	100	800	435
8	18	0.250	X60	100	100	800	435
9	24	0.250	X60	536	89	626	285
10	24	0.250	X60	536	89	626	285
11	24	0.250	X60	536	89	626	285
12	30	0.375	Gr. B	536	89	626	285
13	30	0.375	Gr. B	536	89	626	285
14	36	0.375	Gr. B	447	74	521	226
15	36	0.375	Gr. B	447	74	521	226

4.9.2 Rebound Behavior

The rebound characteristics of unrestrained dent Types A and BH are graphed to show how well the models performed. Of the fifteen test specimens, six were modeled with identical pipe sizes, pipe grades, dent types, dent depths, and pressure histories. The test specimens modeled identically are:

- Specimen 9 with Type A dents
- Specimen 10 with Type BH dents
- Specimen 12 with Type A dents
- Specimen 13 with Type BH dents
- Specimen 14 with Type A dents
- Specimen 15 with Type BH dents

Specimen 9 was tested with unrestrained Type A dents with initial dent depths of 5, 7.5, and 10 percent *d/D*. The rebound behavior of Specimen 9 and the corresponding model is given in Fig. 4-143. The dent depths were measured in the center of the dent on the bulge. Specimen 9 is Grade X60. It was tested assuming a stress distribution of X42. The model was given the same grade and pressure history as the specimen. Due to the location of measurement on the bulged dents, all final depth measurements are similar for the different initial dent depths. The rebound of the model is similar to the rebound of the specimen.

Specimen 10 was tested with unrestrained Type BH dents with initial dent depths of 5 and 10 percent *d/D*. The rebound behavior of Specimen 10 is given in Fig. 4-144. The properties of Specimen 10 are identical to those of Specimen 9. The initial and final rebound dent depths are similar between the model and specimen. The shape of the specimen curves suggests that the initial depths were higher than recorded due to inaccuracies in depth measurement during indentation caused fiom deflection of the load frame and deformation of the supporting saddle.

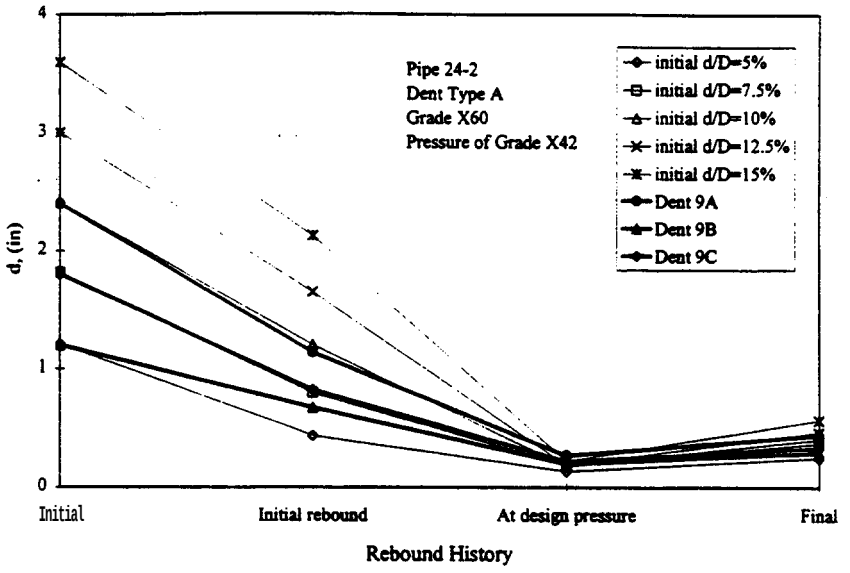

Figure 4-143: Rebound behavior of Specimen 9 (Pipe 24-2 dent Type A).

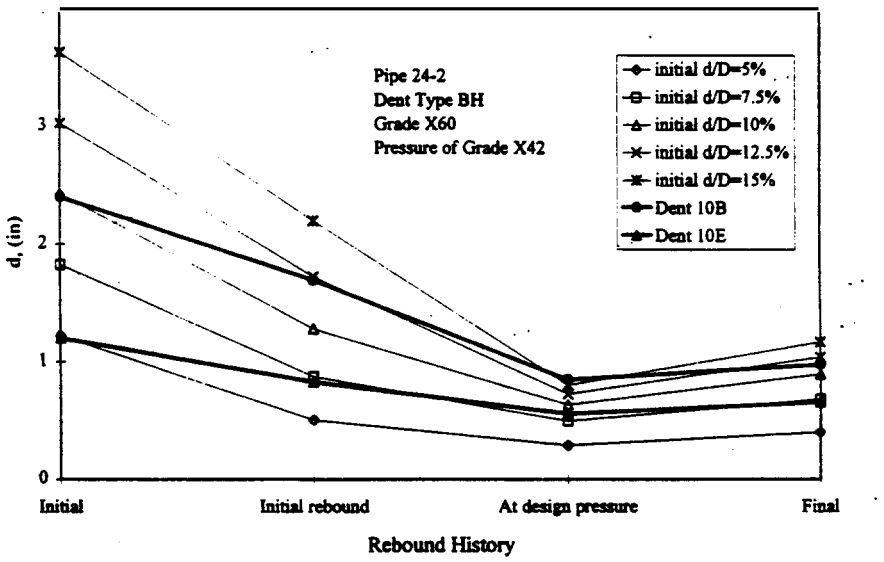

Figure 4-144: Rebound behavior of Specimen 10 (Pipe 24-2 dent Type BH).

Specimens 12 and 13 are given in Fig. 4-145 and 4-146, respectively. The rebound behavior for the Type A dents was similar for the experimental dents and modeled dents. The initial and final rebound data for the Type BH dents are comparable between the specimen and model. As with Specimen 10, the initial dent depths for Specimen 13 are likely higher than recorded.

Specimens 14 and 15 are given in Fig. 4-147 and 4-148, respectively. The rebound characteristics of the specimens and model are comparable for both dent types. The initial depth of the deepest experimental Type A dent may have been lower than recorded. For the six comparisons, the rebound characteristics of the models are reasonably close to actual values fiom the experimental specimens. The models have slightly higher final dent depths suggesting an artificial stiffness inherent to the models. For the nonlinear large displacement elasto-plastic modeling, the models used in this parametric study give acceptable rebound behavior. Thus, the rebound behavior of dents can be determined with finite element modeling with a level of confidence such that experimental testing is not necessary.

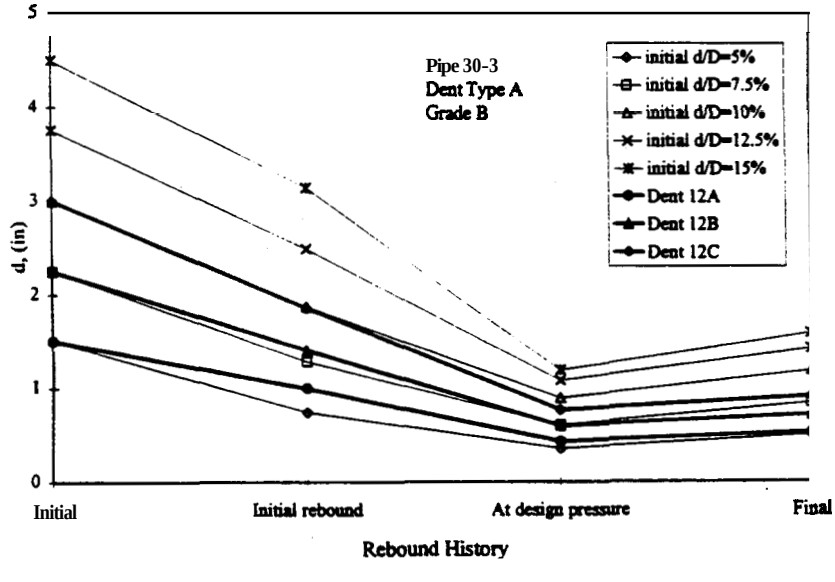

Figure 4-145: Rebound behavior of Specimen 12 (Pipe 30-3 dent Type A).

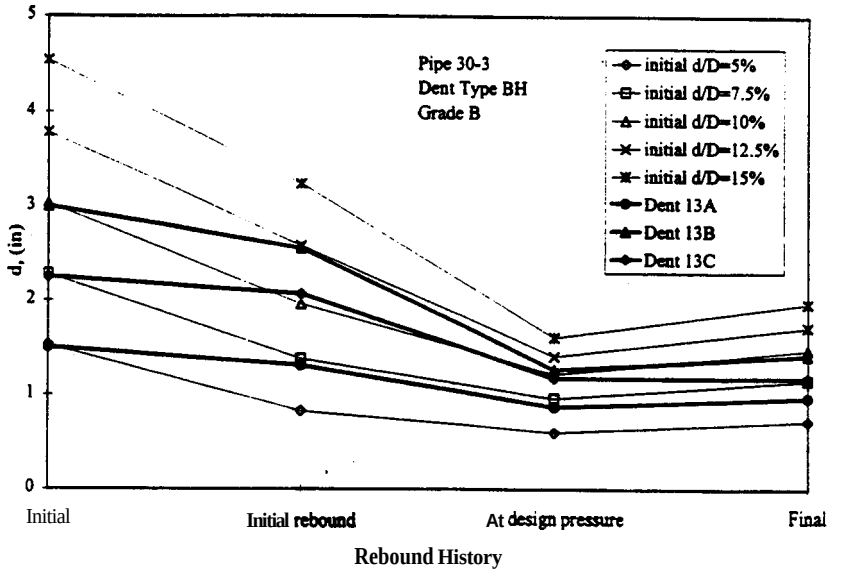

Figure 4-146: Rebound behavior of Specimen 13 (Pipe 30-3 dent Type BH).

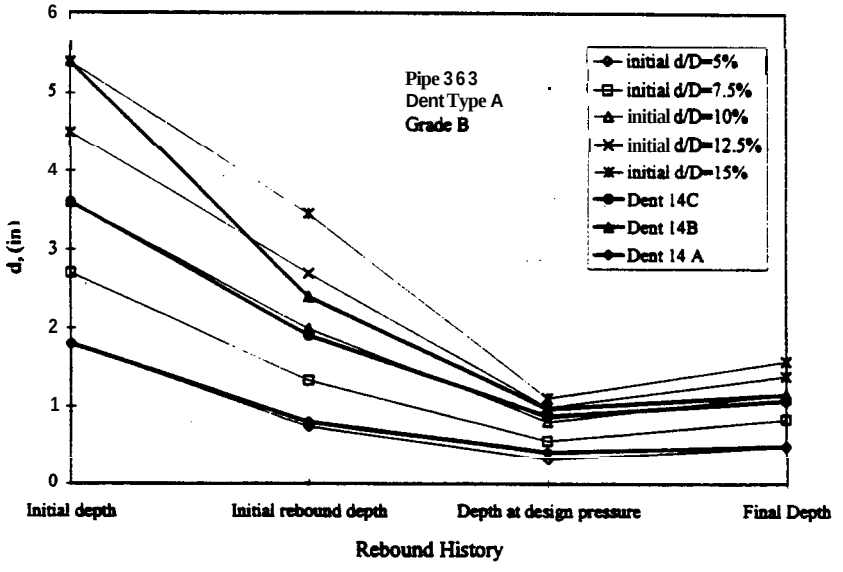

Figure 4-147: Rebound behavior of Specimen 14 (Pipe 36-3 dent Type A).

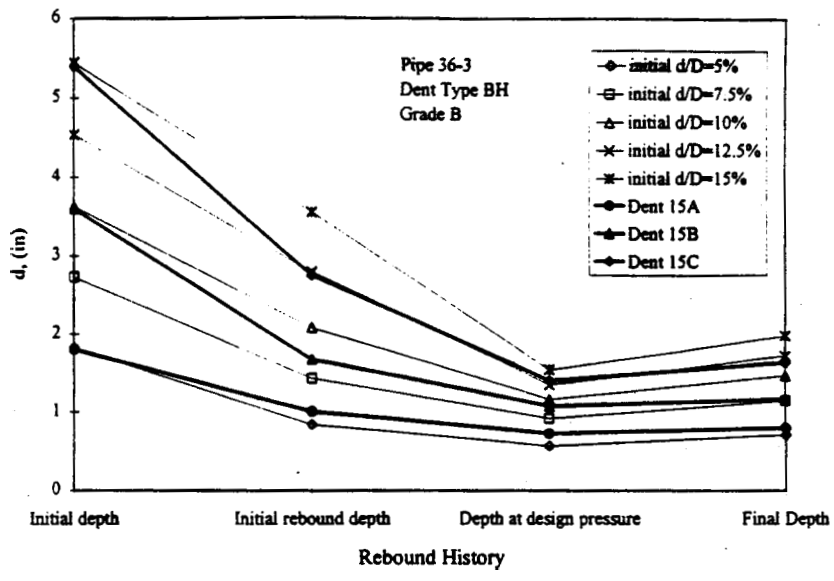

Figure 4-148: Rebound behavior of Specimen 15 (Pipe 36-3 dent Type BH).

4.9.3 Failure Modes

The failure modes predicted with the models are compared to actual failures from the experimental specimens for unrestrained dents Type A and BH. The failure data from the experimental program is given in Tables 4-24 for unrestrained longitudinal Type A dents tested. These dents were tested with defects in the contact region. Longitudinal grooves or scratches were placed for the full length of the contact region prior to indentation. The grooves simulated gouges. They were machined into the pipe wall. The grooves were found to severely affect the fatigue behavior. Scratches were used to create defects of less severity. Scratches were manually scribed into the pipe with a carbon tipped scribe. The failure data for Type BH dents experimentally tested is given in Table 4-25. No initial defects were experimentally tested with Type BH dents.

The mode of failure for the experimentally tested dents is primarily influenced by indenter length. All but two Type **A** dents exhibited failure Mode 1. The two exceptions had failure Mode 2. All Type BH dents exhibited failure Mode 2.

Table **4-24:** Experimental dent Type A failure ***summary.***

Dent ID	Dent Type	Initial Defect	Initial *d/D* (%)	Fatigue Failure	Cyclesto Failure	Failure Mode
1-A	A	groove	5.0	Yes	94,559	1
1-B	A	groove	15.0	Yes	33,521	1
1-C	A	groove	10.0	Yes	27.03 1	1
4-A	A	groove	5.0	Yes	44,286	1
4-B	A	groove	18.8	Yes	2,515	1
4-C	A	groove	10.0	Yes	7,600	1
4-D	A	groove	15.0	Yes	2,515	1
6-E	A	scratch	5.0	Yes	21,541	1
6-F	A	scratch	10.0	Yes	8,349	1
6-G	A	scratch	7.5	Yes	11,791	1
6-H	A	scratch	15.0	Yes	3,785	1
9-A	A	scratch	10.0	Yes	12,711	1
9-B	A	scratch	5.0	Yes	30,108	1
9-C	A	scratch	7.5	Yes	18,608	1
12-A	A	scratch	5.0	Yes	44,484	1
12-B	A	scratch	7.5	Yes	60,891	1
12-c	A	scratch	10.0	No	100,891	1
14-A	A	scratch	5.0	Yes	79,925	1
14-B	A	scratch	10.0	Yes	101,125	2
14-C	A	scratch	15.0	No	101,125	2

Table **4-25:** Experimental dent Type BH failure ***summary.***

Dent ID	Dent Type	Initial Defect	Initial *d/D* (%)	Fatigue Failure	Cycles to Failure	Failure Mode
2-A	BH-L	none	7.5	No	128,732	2
2-B	BH-L	none	10.0	No	128,732	2
2-C	BH-L	none	12.5	No	128,732	2
2-E	BH-L	none	17.5	No	128,732	2
2-1	BH-L	none	15.0	No	128,732	2
3-A	BH-T	none	5.0	No	100,943	2
3-B	BH-T	none	7.5	No	100,943	2
3-C	BH-T	none	10.0	No	100,943	2
3-D	BH-T	none	12.5	Yes	89,684	2
3-E	BH-T	none	15.0	Yes	80,880	2
5-A	BH-T	none	5.0	No	98,079	2
5-B	BH-T	none	10.0	Yes	98,079	2
5-C	BH-T	none	15.0	No	98,079	2
5-D	BH-L	none	10.0	Yes	62,970	2
5-E	BH-L	none	15.0	Yes	73,977	2
7-A	BH-L	none	7.5	No	103,100	2
7-B	BH-L	none	10.0	No	103,100	2
7-c	BH-L	none	12.5	No	103,100	2
7-E	BH-L	none	17.5	No	103, 100	2
7-1	BH-L	none	15.0	No	103,100	2
8-B	BH-T	none	15.0	No	101,587	2
8-D	BH-T	none	17.5	No	101,587	2
10-A	BH-T	none	10.0	No	109,332	2
10-B	BH-L	none	10.0	Yes	101,282	2
10-c	BH-T	none	7.5	No	109,332	2
10-D	BH-T	none	5.0	No	109,332	2
10-E	BH-L	none	5.0	No	109,332	2
12-A	BH-L	none	5.0	No	100,050	2
12-B	BH-L	none	10.0	No	100,050	2
12-c	BH-L	none	7.5	No	100,050	2
14-A	BH-L	none	5.0	No	111,425	2
14-B	BH-L	none	10.0	No	111,425	2
14-c	BH-L	none	15.0	Yes	111,425	2

Failure modes for unrestrained longitudinal dents of Type A and BH are given in Tables 4-11 and 4-12 for the models. These failure modes were directly compared to the failure modes from the experimental program. The experimentally tested and modeled Type BH dents all exhibit Mode 2 failure. The shallow 5 percent d/D Type BH dents modeled were predicted to have failure Mode 1. No fatigue cracks developed for the shallow Type BH dents in the experimental test program. They were assumed to have failure Mode 2.

The modeled Type A dents give identical failure modes as in the experimental program for dents in specimens with diameters up to 24 in. All of these dents have Mode 1 failure. The transition of failure mode from Mode 1 to Mode 2 occurs in the 30 in. and 36 in. pipes. The three experimental Type A dents for the 30 in. diameter pipe (Specimen 12) all had Mode 1 fatigue cracks. The models predict these failure modes. The two shallowest dents were predicted to have Mode 1 failure. The deeper 10 percent d/D dent was predicted to have either failure Mode 1 or 2 where Mode 2 was assumed to be the most probable mode. The scratch in the contact region was not accounted for in the modeling. It provides initial damage making Type A dents more susceptible to Mode 1 failures, as compared to Type A dents without initial damage.

Both failure modes were observed for Type A dents in the 36 in. pipe (Specimen 14). The shallowest dent had a Mode 1 failure. The deeper dents developed peripheral cracks defined as Mode 2 failure. The models give identical results for the three initial dent depths with predicted failure Mode 1 for the shallow dent and Mode 2 for the deeper dents.

The failure modes predicted with the finite element modeling were identical to the failures found in the experimental program. The predicted failure modes are based on stress range data from the models. The similarity of the failure modes verifies that the finite element models give acceptable results for determining fatigue failure modes of dents.